

# Acid ceramidase as a therapeutic target in metastatic prostate cancer<sup>S</sup>

Luz Camacho,<sup>1,\*</sup> Óscar Meca-Cortés,<sup>†</sup> José Luis Abad,<sup>\*</sup> Simón García,<sup>†</sup> Nuria Rubio,<sup>§</sup> Alba Díaz,<sup>\*\*</sup> Toni Celià-Terrassa,<sup>†</sup> Francesca Cingolani,<sup>\*</sup> Raquel Bermudo,<sup>\*\*\*,††</sup> Pedro L. Fernández,<sup>\*\*\*,††,§§,\*\*\*\*</sup> Jerónimo Blanco,<sup>§</sup> Antonio Delgado,<sup>\*\*\*,†††</sup> Josefina Casas,<sup>\*</sup> Gemma Fabriàs,<sup>2,\*\*</sup> and Timothy M. Thomson<sup>2,†</sup>

Department of Biomedical Chemistry, Research Unit on Bioactive Molecules (RUBAM),<sup>\*</sup> Institute for Advanced Chemistry of Catalonia, National Research Council (IQAC-CSIC), Barcelona, Spain; Department of Cell Biology,<sup>†</sup> Molecular Biology Institute of Barcelona, National Research Council (IBMB-CSIC), Barcelona, Spain; Cardiovascular Research Center, National Research Council (ICCC-CSIC),<sup>§</sup> CIBER-BBN, Barcelona, Spain; Tumor Bank,<sup>\*\*</sup> Hospital Clínic and Institut d'Investigacions Biomèdiques August Pi i Sunyer (IDIBAPS) Biobank, Barcelona, Spain; Human and Experimental Functional Oncomorphology Group,<sup>††</sup> Institut d'Investigacions Biomèdiques August Pi i Suner (IDIBAPS), Barcelona, Spain; Department of Pathology,<sup>§§</sup> Hospital Clínic, Barcelona, Spain; and School of Medicine<sup>\*\*\*</sup> and Unit of Medicinal Chemistry,<sup>†††</sup> Faculty of Pharmacy, University of Barcelona (UB), Barcelona, Spain

**Abstract** Acid ceramidase (AC) catalyzes the hydrolysis of ceramide into sphingosine, in turn a substrate of sphingosine kinases that catalyze its conversion into the mitogenic sphingosine-1-phosphate. AC is expressed at high levels in several tumor types and has been proposed as a cancer therapeutic target. Using a model derived from PC-3 prostate cancer cells, the highly tumorigenic, metastatic, and chemoresistant clone PC-3/Mc expressed higher levels of the AC *ASAHI* than the nonmetastatic clone PC-3/S. Stable knockdown of *ASAHI* in PC-3/Mc cells caused an accumulation of ceramides, inhibition of clonogenic potential, increased requirement for growth factors, and inhibition of tumorigenesis and lung metastases. We developed de novo *ASAHI* inhibitors, which also caused a dose-dependent accumulation of ceramides in PC-3/Mc cells and inhibited their growth and clonogenicity. Finally, immunohistochemical analysis of primary prostate cancer samples showed that higher levels of *ASAHI* were associated with more advanced stages of this neoplasia. **□** These observations confirm *ASAHI* as a therapeutic target in advanced and chemoresistant forms of prostate cancer and suggest that our new potent and specific AC inhibitors could act by counteracting critical growth properties of

these highly aggressive tumor cells.—Camacho, L., O. Meca-Cortés, J. L. Abad, S. García, N. Rubio, A. Díaz, T. Celià-Terrassa, F. Cingolani, R. Bermudo, P. L. Fernández, J. Blanco, A. Delgado, J. Casas, G. Fabriàs, and T. M. Thomson. **Acid ceramidase as a therapeutic target in metastatic prostate cancer.** *J. Lipid Res.* 2013. 54: 1207–1220.

**Supplementary key words** ceramide • metastasis • inhibitors

Cancer cells develop a lipogenic phenotype that supports the energy and membrane synthesis requirements associated with the enhanced proliferation and survival under stress inherent to malignant progression (1, 2). The recognition of the importance of this phenotype in cancer has led to the use of enzymes of lipid metabolism as markers to monitor neoplastic progression and response to therapy, as well as to the development of drugs targeted at key lipogenic enzymes, such as fatty acid synthase (FASN) (2, 3). The excess fatty acid synthesis that results from the coordinated activation of lipogenic enzymes in many types of cancer leads to the accumulation of palmitate, which needs to be further processed by the cells due to the toxic effects of its accumulation. One pathway that

This work was supported by Ministry of Science and Innovation Grants SAF2008-00706 and SAF2011-22444 (to G.F.); Agència de Gestió d'Ajuts Universitaris i de Recerca de la Generalitat de Catalunya Grant 2009SGR1072 (to G.F.); Ministry of Science and Innovation Grants SAF2008-04136-C02-01 and SAF2011-24686 (to T.M.T.); Ministry of Economy and Competitiveness Grant SAF2012-40017-C02-01 (to T.M.T.); Agència de Gestió d'Ajuts Universitaris i de Recerca de la Generalitat de Catalunya Grant 2009SGR1482 (to T.M.T.); Xarxa de Bancs de Tumors de Catalunya-Pla Director d'Oncologia and Fondo Europeo de Desarrollo Regional (FEDER), Unión Europea "Una manera de hacer Europa" and Ministry of Economy and Competitiveness Grant SAF2012-40017-C02-02 (to P.L.F.); Red Nacional de Biobancos (ReTBioH) (to P.L.F. and R.B.); Generalitat de Catalunya Grant 2009SGR1072 (to L.C.); Ministry of Science and Innovation FPU fellowship (to O.M.C.); I3P fellowship (CSIC) (to T.C-T.); and Generalitat de Catalunya FI fellowship (to F.C.).

Manuscript received 19 September 2012 and in revised form 8 February 2013.

Published, JLR Papers in Press, February 18, 2013  
DOI 10.1194/jlr.M032375

Abbreviations: AC, acid ceramidase; CMH, ceramide monohexoside; MDR1, multidrug resistant protein 1; NC, neutral ceramidase; PC, prostate cancer; PIN, prostate intraepithelial neoplasia; S1P, sphingosine-1-phosphate.

<sup>1</sup> Present address of L. Camacho: Universidad Nacional Autónoma de México, Facultad de Química, Mexico City, DF, Mexico.

<sup>2</sup> To whom correspondence should be addressed.

e-mail: titbmc@ibmb.csic.es (T.M.T.); gemma.fabriàs@iqac.csic.es (G.F.)

**S** The online version of this article (available at <http://www.jlr.org>) contains supplementary data in the form of two tables and four figures.

many neoplastic cells activate to offset the toxic accumulation of palmitate is its peroxisome proliferator-activated receptor (PPAR) $\gamma$ -dependent funneling to eventually form triglycerides, which can be further used as energy stores (4). A second pathway followed by palmitate is the condensation of palmitoyl CoA with L-serine, leading to the synthesis of ceramides (5). The accumulation of ceramides also poses a problem for cell survival because of its proapoptotic consequences (6–8). This can be counteracted by activities that convert ceramides to a variety of metabolites, including sphingosines through deacylation catalyzed by ceramidases. Sphingosines can be converted into the growth- and survival-promoting sphingosine-1-phosphate (S1P) through the action of sphingosine kinases (8). S1P can be either irreversibly degraded by S1P lyase or reutilized by sequential dephosphorylation and acylation for ceramide synthesis. The importance of ceramidases in the context of cancer is supported by the observation that their inhibition by drugs or RNAi severely compromises the growth and survival under stress of tumor cells (9).

De novo ceramide biosynthesis requires the coordinate action of serine palmitoyl transferase and ceramide synthase to generate ceramide. This process begins with the condensation of serine and palmitoyl-CoA to form 3-ketosphinganine (5), which is reduced to the sphingoid base sphinganine and acylated by ceramide synthase to generate dihydroceramide. This compound is oxidized to ceramide by introduction of a *trans*-4,5 double bond. This pathway can be stimulated by drugs and ionizing radiation and usually results in a prolonged ceramide accumulation (10).

Once generated, ceramide may amass or be converted into a variety of metabolites. Phosphorylation by ceramide kinase (11) generates ceramide 1-phosphate, while deacylation by alkaline, neutral or acid ceramidases (the products of different genes) (12) yields sphingosine, which may be phosphorylated by sphingosine kinase to S1P. Two distinct sphingosine kinases have been cloned. These two isoforms differ in temporal patterns of expression during development, are expressed in different tissues, and possess distinct kinetic properties (13), implying that they perform different cellular functions. Ceramide may also be converted back to SM by transfer of phosphorylcholine from phosphatidylcholine via SM synthases (14). Alternatively, it can be glycosylated by glucosylceramide synthase to form glucosylceramide, which may be further modified by various enzymes in the Golgi apparatus to form complex glycosphingolipids (15).

Many tumor types express high levels of acid ceramidase (AC). Specifically, the expression levels of AC in prostate cancer have been reported to be elevated relative to normal prostate tissue (16, 17). Prostate cancer (PC) is the most prevalent neoplasia in men in industrialized nations (18). Although PC is frequently initially sensitive to hormonal deprivation therapies and follows indolent clinical courses, a significant proportion of cases eventually become resistant to such therapeutic approaches, accompanied with aggressive growth, establishment of metastasis, and tumors that are highly resistant to conventional

chemotherapeutic regimes (19, 20). Two major challenges in PC are to find predictive markers that identify those tumors most likely to follow a hormone-independent, aggressive clinical course as aids to decide early intervention and to identify molecular targets for improved therapies of castration-resistant cases that respond poorly to conventional chemotherapeutic regimes. Here, we provide new evidence to reinforce the notion that the acid ceramidase ASAHI is a valid therapeutic target in advanced prostate cancer, and we characterize new potent and specific inhibitors of AC.

## METHODS

### Cells and reagents

PC-3/Mc and PC-3/S cells (21) were grown in RPMI1640 medium supplemented with 10% fetal bovine serum, nonessential amino acids, 2 mM glutamine, 1 mM sodium pyruvate, 100 U/ml penicillin, and 100  $\mu$ g/ml streptomycin (all from PAA, Ontario, Canada). Fibroblasts from a Farber patient (FD, wild-type) and FD transformed to stably overexpress AC (FD10X) were grown in a humidified 5% CO<sub>2</sub> atmosphere at 37°C in DMEM medium supplemented as above.

### Transient transfection of fibroblasts

Twenty-four hours before transfection, cells were plated at a density of  $2.5 \times 10^5$  cells in 35 mm diameter plates. Cells were then transfected with the specific constructs or empty vectors using lipofectamine 2000 (Invitrogen, Carlsbad, CA). Twenty-four hours after transfection, cells were either processed immediately or collected by trypsinization, washed twice with PBS, and centrifuged. Pellets were stored at  $-20^\circ\text{C}$  until use. In transfections with neutral ceramidase (NC), the success of transfection was confirmed by activity assays with CerC12NBD in intact cells.

### Fluorogenic ceramidase assay

Cells were collected by trypsinization, washed with PBS, resuspended in 0.25 M sucrose and lysed by ultrasonication in an ultrasonic bath. For the assay, 75  $\mu$ l of reaction buffer (100 mM sodium acetate buffer, pH 4.5, for acid ceramidase activity), containing 40  $\mu$ M RBM14C12 fluorogenic substrate (22) (with or without test compounds), was mixed with 25  $\mu$ l of the cell lysates (20  $\mu$ g of total protein content) and incubated at 37°C for 3 h. For time dependence of inhibition, incubations were carried out for 0.5, 1, 2, and 3 h with different amounts of protein. The reaction was stopped by addition of methanol followed by NaIO<sub>4</sub> (2.5 mg/ml in 200 mM glycine/NaOH buffer, pH 10.6). After 1 h at 37°C, 100  $\mu$ l of 200 mM glycine/NaOH buffer were added and fluorescence detected at 355/460 nm excitation/emission wavelengths on a SpectraMax Microplate Reader (Molecular Devices, Sunnyvale, CA). To determine ceramidase activity in intact cells,  $2 \times 10^4$  cells/well were seeded in 96-well plates (Nunc, Roskilde, Denmark). The following day, medium was replaced by 100  $\mu$ l fresh medium containing 40  $\mu$ M RBM14C12 fluorogenic substrate incubated for 3 h at 37°C in a 5% CO<sub>2</sub> atmosphere, and the assay was continued as above.

### Papain activity

Papain activity was determined in 96-well plates by a modification of the reported procedure (23). The reaction mixture contained 250  $\mu$ l of 0.1 M phosphate buffer (pH 6.5) with 0.3 M KCl, 0.1 mM EDTA, and 3 mM DTT; 30  $\mu$ l of substrate solution (L-pyroglyutamyl-L-phenylalanyl-L-leucine-*p*-nitroanilide; 2.2 mM

in DMSO, 0.22 mM final concentration); 20  $\mu$ l of enzyme solution (30  $\mu$ g/ml in reaction buffer); and 3  $\mu$ l of inhibitor solution or vehicle. Chymostatin at 1  $\mu$ M and 10  $\mu$ M was used as positive control of inhibition of papain activity. The reaction was stopped by the addition of 20  $\mu$ l of 1 N HCl, and the OD was measured at 410 nm.

### Sphingolipid analysis by UPLC/MS

The liquid chromatography-mass spectrometry equipment consisted of a Waters Aquity UPLC system connected to a Waters LCT Premier orthogonal accelerated time of flight mass spectrometer (Waters, Millford, MA), operated in positive electrospray ionization mode. Full scan spectra from 50 to 1,500 Da were acquired, and individual spectra were summed to produce data points every 0.2 s. Mass accuracy and reproducibility were maintained by using an independent reference spray by the LockSpray interference. The analytical column was a 100 mm  $\times$  2.1 mm id, 1.7  $\mu$ m C8 Acquity UPLC BEH (Waters). The two mobile phases were phase A: MeOH/H<sub>2</sub>O/HCOOH (74:25:1 v/v/v); phase B: MeOH/HCOOH (99/1 v/v), both also containing 5 mM ammonium formate. A linear gradient was programmed as follows: 0.0 min: 80% B; 3 min: 90% B; 6 min: 90% B; 15 min: 99% B; 18 min: 99% B; 20 min: 80% B, at 0.3 ml/min flow rate. The column was held at 30°C. Quantification was carried out using the extracted ion chromatogram of each compound, using 50 mDa windows. Linear dynamic range was determined by injecting standard mixtures, and positive identification of compounds was based on accurate mass measurement (< 5 ppm error) and LC retention time compared with that of a standard ( $\pm$  2%).

### HPLC/fluorescence detection

These analyses were carried out in an Alliance Waters 2695 HPLC system coupled to a Waters 2475 Multi  $\lambda$  fluorescence detector (Waters, Milford USA) equipped with an Atlantis T3 C18 (50 mm  $\times$  4.6 mm) column (Waters). The mobile phase was composed of a mixture of acetonitrile/H<sub>2</sub>O (80:20), and the flow rate was set at 1 ml/min. All solvents contained 0.1% trifluoroacetic acid. Fluorescent compounds were monitored at 420/483 nm excitation/emission wavelengths. Peak quantification was carried out using the Empower Pro 2.0 software (Waters).

### Western blotting

Cells were lysed (10 mM Tris-HCl, pH 7.4, 100 mM NaCl, 1 mM EDTA, 1 mM EGTA, 1 mM NaF, 20 mM Na<sub>4</sub>P<sub>2</sub>O<sub>7</sub>, 2 mM Na<sub>3</sub>VO<sub>4</sub>, 1% Triton-X 100, 10% glycerol, 0.1% SDS, 0.5% deoxycholate, 1 mM PMSF, 1 mg/ml aprotinin, and leupeptin), proteins separated by SDS-polyacrylamide electrophoresis (Bio-Rad Laboratories, Hercules, CA) and transferred to nitrocellulose membrane blots (Bio-Rad). After blocking with 5% nonfat milk in PBS containing 0.1% Tween 20, membranes were incubated with primary antibody, washed, incubated with HRP-conjugated goat anti-rabbit IgG or anti-mouse IgG antibodies, and then washed again. Signals were detected by chemoluminescence (ECL Western Blotting Detection Kit, Amersham Biosciences, Barcelona, Spain). Actin signals were used as protein loading and transfer references.

### Real-time RT-PCR

Total RNA was extracted with the RNeasy Kit (Qiagen, Venlo, Netherlands). Complementary DNAs were synthesized with the High-Capacity cDNA Reverse Transcription Kit (Applied Biosystems, Foster City, CA). Real-time quantitative PCR assays were performed on a LightCycler 480 instrument (Roche Diagnostics, Mannheim, Germany) and analyzed with the LightCycler

480 Software release 1.5.0. The amplification levels of RN18S1 and HMBS were used as internal references to estimate the relative levels of specific transcripts, and relative quantification was determined by the  $\Delta\Delta C_p$  method. All determinations were done in triplicate.

### Cell cycle analysis

Cells were seeded in 6-well Corning plates (Corning, NY), detached with Trypsin/EDTA/1% BSA, washed twice, resuspended in PBS, and fixed at 4°C for at least 2 h by dropwise addition of 70% ethanol. Subsequently, cells were washed with PBS/50 mM EDTA/1% BSA and incubated with 1 mg/ml RNase A (Sigma) at 37°C for 1 h and 0.1 mg/ml propidium iodide (Sigma, Alcobendas, Madrid, Spain). DNA content was determined in a Cytomics FC500 instrument (Coulter, Hialeah, FL), and cell cycle distribution analyzed with Multicycle. All determinations were done in triplicate.

### Anchorage-independent growth

For soft-agar colony formation assays, 0.5% agar in complete culture medium was placed at the bottom of 12-well plates, allowed to solidify, and overlaid with a suspension of  $3 \times 10^3$  cells in 0.3% agar in complete medium. After solidification, wells were fed with complete medium twice a week. After three weeks, they were fixed with 0.5% glutaraldehyde, stained with 0.025% crystal violet, and visualized under a Leica magnifying glass (Wetzler, Germany) coupled to an Olympus digital camera (Olympus, Hamburg, Germany). Colonies  $\geq$  0.2 mm diameter were scored with the ImageJ software (National Institutes of Health, MD). Each experimental condition was performed in triplicate.

### In vivo tumor formation

For localized growth,  $1 \times 10^3$  to  $1 \times 10^5$  cells with stably integrated firefly luciferase were injected in a volume of 50  $\mu$ l of RPMI 1640 (without FBS) intramuscularly in each hind limb of anesthetized six-week-old male NOD-SCID mice. Tumor growth was monitored by luminometry on an ORCA-2BT instrument (Hamamatsu Photonics, Hamamatsu, Japan), 5 min after intraperitoneal injection of luciferine (100 mg/kg in 150  $\mu$ l of PBS). For lung colony formation,  $5 \times 10^5$  cells in 150  $\mu$ l RPMI1640 were injected through the dorsal caudal vein. Mice were imaged immediately after injection, and thereafter, tumor development was monitored by weekly imaging. For bioluminescence plots, photon flux was calculated relative to background values from luciferin-injected mice with no tumor cells and normalized to the value obtained immediately after xenografting. In lung colonization free survival analysis, lesions that had an increased photon flux value above day 0 were counted as events.

### Production and transduction of lentiviral particles

Constructs based on the pLKOpuromycin vector and bearing ASAH1-targeting shRNAs or control sequences were purchased from Sigma-Aldrich. The lentivirus packaging cell line HEK293T was cotransfected with these DNAs, together with pCMVdeltaR8.91 and pVSV-G (Clontech, Mountain View, CA) for 12 h using Eugene HD (Roche). Supernatants were collected for the following 48 h and filtered through 0.45  $\mu$ m methylcellulose filters (Millipore, Billerica, MA). Lentiviral particles were concentrated by ultracentrifugation at 27,000 rpm for 90 min on 20% sucrose density gradients. Viral particles were resuspended with medium and added to the cells together with 8  $\mu$ g/ml polybrene (Sigma). Cells were infected for 24 h and allowed to recover in fresh medium for 24–48 h. Selection for cells with integrated sequences was carried out for three days in medium supplemented with 5  $\mu$ g/ml puromycin (Biomol, Exeter, UK).

## Cell viability assay

MTT (3-(4,5-Dimethylthiazol-2-yl)-2,5-diphenyltetrazolium bromide, Sigma) was added to cultured cells at a final concentration of 0.5 mg/ml, incubated at 37°C for 3 h, and the resulting precipitates were solubilized with dimethyl sulfoxide. Absorbance was measured at 570 nm on a SpectraMax Microplate Reader (Molecular Devices, Sunnyvale, CA).

## Synthesis of novel acid ceramidase inhibitors

A solution of 1-hydroxybenzotriazole (18 mg, 0.13 mmol), the corresponding carboxylic acid (0.1 mmol), and *N*-(3-dimethylaminopropyl)-*N*'-ethylcarbodiimide hydrochloride (20 mg, 0.13 mmol) in CH<sub>2</sub>Cl<sub>2</sub> (1 ml) was added to a mixture containing sphinganine (30 mg, 0.1 mmol), NEt<sub>3</sub> (30 μl, 0.2 mmol) in THF or CH<sub>3</sub>CN (1 ml). The resulting solution was stirred for 1 h at room temperature and concentrated at reduced pressure. The residue was taken up in CH<sub>2</sub>Cl<sub>2</sub> (2 ml), washed with saturated aqueous NaHCO<sub>3</sub> solution (3 × 0.5 ml), and then the solvent was evaporated to give a crude mixture that was purified by flash chromatography on silica gel using a gradient of 0–5% CH<sub>2</sub>Cl<sub>2</sub>/MeOH to afford the pure amide in 70–85% yield.

Spectroscopic data for the synthesized compounds: SABRAC: *N*-[(2*S*,3*R*)-1,3-dihydroxyoctadecan-2-yl]2-bromoacetamide. <sup>1</sup>H-NMR (400 MHz, CDCl<sub>3</sub>): 7.40 (1H, NH), 4.20 (2H), 4.05 (1H), 3.85 (1H), 3.83 (1H), 3.81 (1H), 1.55 (2H), 1.25–1.30 (26H), 0.88 (t, 3H). <sup>13</sup>C-NMR (101 MHz, CDCl<sub>3</sub>): 177.2, 74.2, 62.2, 54.0, 42.8, 34.7, 32.0, 29.8–29.6, 26.0, 22.8, 14.3. RBM1-12: *N*-[(2*S*,3*R*)-1,3-dihydroxyoctadecan-2-yl]2,2-dibromoacetamide. <sup>1</sup>H-NMR (400 MHz, CD<sub>3</sub>OD): 6.23 (1H, NH), 3.80 (1H), 3.75 (2H), 3.65 (1H), 1.44 (2H), 1.25–1.30 (26H), 0.90 (3H). <sup>13</sup>C-NMR (101 MHz, CD<sub>3</sub>OD): 166.9, 71.9, 61.7, 57.6, 37.9, 34.9, 33.1, 30.8–30.5, 26.6, 23.7, 14.5. RBM1-13: *N*-[(2*S*,3*R*)-1,3-dihydroxyoctadecan-2-yl]2-methylacrylamide. <sup>1</sup>H-NMR (400 MHz, CDCl<sub>3</sub>): δ 6.75 (1H, NH), 5.72 (1H), 5.38 (1H), 4.05 (1H), 3.87 (1H), 3.81 (2H), 1.99 (3H), 1.42 (2H), 1.25–1.35 (26H), 0.88 (3H). <sup>13</sup>C-NMR (101 MHz, CDCl<sub>3</sub>): δ 168.6, 139.7, 120.2, 74.2, 62.3, 53.7, 32.7, 31.8, 29.9–29.3, 25.9, 22.7, 14.1. RBM1-15: (*E*)-4-[(2*S*,3*R*)-*N*1,3-dihydroxyoctadecan-2-ylamino]4-oxo-2-butenic acid. <sup>1</sup>H-NMR (400 MHz, CDCl<sub>3</sub>): δ 7.9 (1H, NH), 6.45 (1H), 6.35 (1H), 4.12 (1H), 3.88 (3H), 1.45 (2H), 1.25 (26H), 0.88 (3H). <sup>13</sup>C-NMR (101 MHz, CDCl<sub>3</sub>): δ 166.4, 166.2, 135.5, 132.5, 73.6, 61.2, 54.7, 34.5, 32.1, 29.8–29.5, 26.1, 22.8, 14.2. RBM1-16: *N*-[(2*S*,3*R*)-1,3-dihydroxyoctadecan-2-yl]3-methyl-2-butenamide. <sup>1</sup>H-NMR (400 MHz, CDCl<sub>3</sub>): δ 6.26 (1H, NH), 5.64 (1H), 4.05 (1H), 3.85 (1H), 3.80 (1H), 2.17 (3H), 1.86 (3H), 1.54 (2H), 1.25 (26H), 0.88 (3H). <sup>13</sup>C-NMR (101 MHz, CDCl<sub>3</sub>): δ 167.4, 151.2, 118.5, 74.3, 62.7, 53.9, 34.7, 32.0, 29.8–29.5, 27.3, 26.1, 22.8, 19.9, 14.2. RBM1-17: (2*E*,4*E*)-*N*-[(2*S*,3*R*)-1,3-dihydroxyoctadecan-2-yl]hexa-2,4-dienamide. <sup>1</sup>H-NMR (400 MHz, CDCl<sub>3</sub>): δ 7.11 (dd, *J* = 14.8 Hz, *J'* = 10 Hz, 1H), 6.90 (1H, NH), 6.05 (2H), 5.78 (d, *J* = 15.2 Hz, 1H), 3.95 (2H), 3.62 (1H), 1.78 (d, *J* = 6 Hz, 3H), 1.45 (2H), 1.19 (26H), 0.82 (3H). <sup>13</sup>C-NMR (101 MHz, CDCl<sub>3</sub>, CD<sub>3</sub>OD): δ 167.3, 141.7, 138.2, 129.7, 121.3, 73.3, 61.9, 54.5, 34.3, 31.9, 29.7–29.3, 26.0, 22.7, 18.5, 14.1. RBM1-18: (*E*)-*N*-[(2*S*,3*R*)-1,3-dihydroxyoctadecan-2-yl]but-2-enamide. <sup>1</sup>H-NMR (400 MHz, CD<sub>3</sub>OD): δ 6.88 (1H), 6.02 (1H), 5.87 (d, *J* = 14.3, 1H), 3.85 (1H), 3.71 (2H), 3.63 (1H), 1.87 (d, *J* = 6.6, 3H), 1.52 (2H), 1.25 (26 H), 0.88 (3H). <sup>13</sup>C-NMR (101 MHz, CD<sub>3</sub>OD): δ 168.5, 140.8, 126.2, 72.5, 62.3, 56.9, 35.0, 33.1, 30.9, 30.7–30.4, 26.9, 23.8, 18.0, 14.6. RBM1-19: *N*-[(2*S*,3*R*)-1,3-dihydroxyoctadecan-2-yl]acrylamide. <sup>1</sup>H-NMR (400 MHz, CDCl<sub>3</sub>): δ 6.33 (d, *J* = 17.0, 1H), 6.17 (dd, *J* = 10.2, 16.9, 1H), 5.69 (d, *J* = 11.1, 1H), 4.16–3.99 (1H), 3.96–3.71 (3H), 1.68–1.46 (4H), 1.25 (24H), 0.88 (3H). <sup>13</sup>C-NMR (101 MHz, CDCl<sub>3</sub>): δ 165.7, 131.0, 127.3, 74.5, 62.4, 54.0, 34.7, 32.1, 30.0, 29.7, 29.5, 26.3, 22.8, 14.2.

## Immunohistochemistry

The procurement of human tissues complied with Spanish legislation regarding informed consent, privacy, and all legal requirements after approval by the Hospital Clínic Institutional Ethics Committee. Sections (2 μm thick) were obtained for immunohistochemistry either from formalin-fixed and paraffin-embedded tissue blocks or from tissue microarrays (TMA) built with a Manual Tissue Arrayer 1 (Beecher Instruments, Sun Prairie, WI). A total of 33 samples, containing normal, prostate intraepithelial neoplasia, and carcinomatous glands were analyzed. Tissue sections were mounted on xy-laned glass slides (Thermo Scientific, Braunschweig, Germany) and used for immunohistochemical staining using the Bond Polymer Refine Detection System (Leica Microsystems, Wetzlar, Germany). Samples were deparaffinized, antigen retrieval was performed at pH 6 for 20 min in citrate buffer, and primary antibody was incubated for 1 h at room temperature. Rabbit anti-ASAHI (BD Transduction Laboratories, Franklin Lakes, NJ) was used at a dilution of 1/100. Staining was scored as the percentage of cells with clear positivity and the predominant staining intensity. Images were captured with an Olympus BX-51 microscope equipped with an Olympus DP70 camera.

## Statistical analysis

Significance was determined by the two-tailed unpaired *t*-test using the Graph Pad Prism 4.0 software.

## RESULTS

### Increased expression of acid ceramidase in highly metastatic clones derived from PC-3 prostate cancer cells

The PC-3 prostate cancer cell line was used to generate two distinct clonal populations. PC-3/S cells were isolated in vitro by single-cell cloning from luciferase-expressing PC-3 cells. A second single-cell progeny, hereafter designated PC-3/Mc, was isolated from luciferase-expressing PC-3/M cells, a PC-3 subline that had been selected in vivo for its high metastatic potential (21). Intramuscular grafting in NOD-SCID mice of 2.5 × 10<sup>5</sup> PC-3/Mc cells quickly produced large tumors (Fig. 1A) with the appearance of abdominal lymph node metastases by 19 days in 50% of mice (21). In vitro, PC-3/Mc cells grew much faster than PC-3/S cells (Fig. 1B). Moreover, PC-3/Mc cells were highly clonogenic, whereas PC-3/S cells showed limited anchorage-independent growth (Fig. 1C).

To investigate the sphingolipid profiles of both cell lines, cells were seeded (0.25 × 10<sup>6</sup> cells/ml) and grown under standard conditions, and their sphingolipid composition determined after 48 h of culture. LC/MS analysis showed that total ceramide abundance in PC-3/S cells was 1.3-fold that of PC-3/Mc cells (Fig. 1D). Interestingly, this difference increased to 2.2 for the C14 and C16 *N*-acyl species (PC-3/S versus PC-3/Mc ratio: 2.2). Likewise, the cell content of SM and ceramide monohexosides (CMH, including both glucosylceramides and galactosylceramides) was 1.3–1.5 times higher in PC-3/S cells than in PC-3/Mc cells (Fig. 1E, F), and this difference was similar for all the differently *N*-acylated species. No significant differences between free bases and

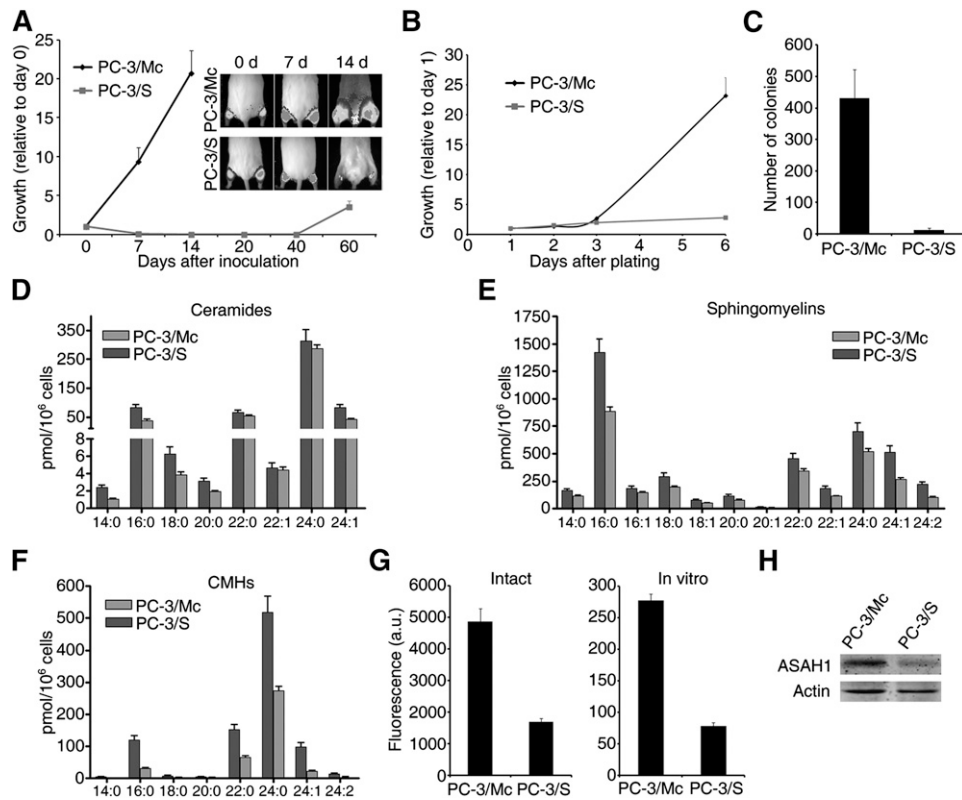


**Fig. 1.** Comparative growth phenotypes and sphingolipid profiles between metastatic PC-3/Mc cells and nonmetastatic PC-3/S cells. **A:** PC-3/Mc cells rapidly grew tumors upon intramuscular inoculation in NOD-SCID mice, as opposed to the very slow tumor growth of PC-3/S cells. **B:** In vitro, PC-3/Mc cells grew at a much faster rate than PC-3/S cells under standard growth conditions on plastic dishes. **C:** PC-3/Mc cells were very efficient at growing colonies under anchorage-independent conditions (soft agar), as opposed to the poorly clonogenic PC-3/S cells. **D–F:** PC-3/Mc cells displayed a lower abundance of ceramides (**D**), sphingomyelins (**E**), and ceramide monohexoses (**F**) than PC-3/S cells. The lower ceramide content in PC-3/Mc cells was statistically significant ( $P \leq 0.05$ ; unpaired, two-tailed *t*-test) for the 14:0, 16:0, 18:0, 20:0, and 24:1 species. All SM and CMH species were present at significantly lower levels in PC-3/Mc cells than in PC-3/S cells. **G:** PC-3/Mc cells displayed significantly higher levels of acid ceramidase activity as compared with PC-3/S cells, assayed using either intact cells or cell lysates. **H:** The acid ceramidase ASAH1 was expressed at significantly higher levels in PC-3/Mc cells than in PC-3/S cells, as determined by Western blotting. Actin signal was used to monitor protein loading and transfer.

long-chain phosphates were detected between the two cell lines (not shown).

Enzyme activity determination showed that the highly aggressive and metastatic PC-3/Mc cells displayed levels of AC activity that were 2.5 to 4 times higher than those of PC-3/S cells, determined either in cell lysates at acidic pH or in intact cells (Fig. 1G) using a fluorogenic assay (22). Several findings support that the bulk of the ceramidase activity detected in these cells is due to AC. First, the fluorogenic substrates were accepted by neutral ceramidase but not by alkaline ceramidases (not shown). Second, RBM14-C8, which is a substrate of NC but not of AC, was not hydrolyzed by PC-3/Mc cells. Third, the hydrolytic activity detected in these cells was lost after treatment with SABRAC, which inhibits AC but not NC (see below). Furthermore, PC-3/Mc cells expressed 2- to 4-fold higher levels of the AC ASAH1 than PC-3/S cells, as determined by Western blotting (Fig. 1H). A comparative transcriptomic survey showed that the observed differences in ASAH1

protein and activity levels were not paralleled by significant differences at the mRNA level (not shown), suggesting a posttranscriptional regulation of ASAH1 expression.

#### Requirement of ASAH1 for optimal growth and metastatic potential of PC-3/Mc cells

Given the above differential ceramidase activity and expression of ASAH1 protein between metastatic and nonmetastatic prostate cancer cell clonal populations and to determine its importance for the growth and metastatic properties of PC-3/Mc cells, we proceeded to stably knock down its transcript. Cells were transduced with five different lentiviral constructs expressing shRNAs targeting five distinct sequences on the ASAH1 mRNA. Three of these shRNAs were effective at specifically decreasing ASAH1 mRNA levels with variable efficacies, ranging from 90 to 60% (Fig. 2A). This gene knockdown was paralleled by a corresponding inhibition of the AC activity in these cells (Fig. 2A). The silencing efficacies

of shRNAs 399 and 402 were confirmed by Western blotting (Fig. 2B).

The sphingolipid content of ASAHI-knockdown PC-3/Mc cells was analyzed by UPLC-TOF. Both ASAHI-specific shRNAs caused the accumulation of ceramides, SM, and CMH compared with cells transduced with a control lentiviral vector (Fig. 2C–E), indicating an impairment of ceramide catabolism, which confirms the functionality of the knockdowns. Unexpectedly, sphingosine was increased in both knockdown clones (Fig. 2F), which suggests that other ceramidases are upregulated upon chronic knockdown of ASAHI (24).

We next tested if this accumulation of ceramides provoked an impairment of the growth or viability of ASAHI-knockdown PC-3/Mc cells. Neither of the two knockdowns had any effect on the PC-3/Mc population, nor did they cause the accumulation of sub-G1 populations, suggesting

that PC-3/Mc cells are resistant to the apoptotic and growth-inhibitory effects of ceramide accumulation under standard growth conditions. Consistently, the growth rate of ASAHI-knockdown PC-3/Mc cells in standard growth medium (10% FBS) did not differ significantly from that of control cells when seeded at initial densities of 1,000 cells/cm<sup>2</sup> (Fig. 3A). However, when seeded at a density of 500 cells/cm<sup>2</sup>, ASAHI-knockdown cells showed a significantly reduced growth rate compared with control cells (Fig. 3B). This suggests that ASAHI might be critically required to sense factors dependent on cell density, including paracrine factors or cell-cell interactions. In order to know whether ASAHI knockdown sensitized PC-3/Mc cells to limiting concentrations of exogenous growth factors, their rate of proliferation was determined in medium containing 0.5% FBS. Under these conditions, ASAHI-knockdown PC-3/Mc cells grew at significantly slower rates

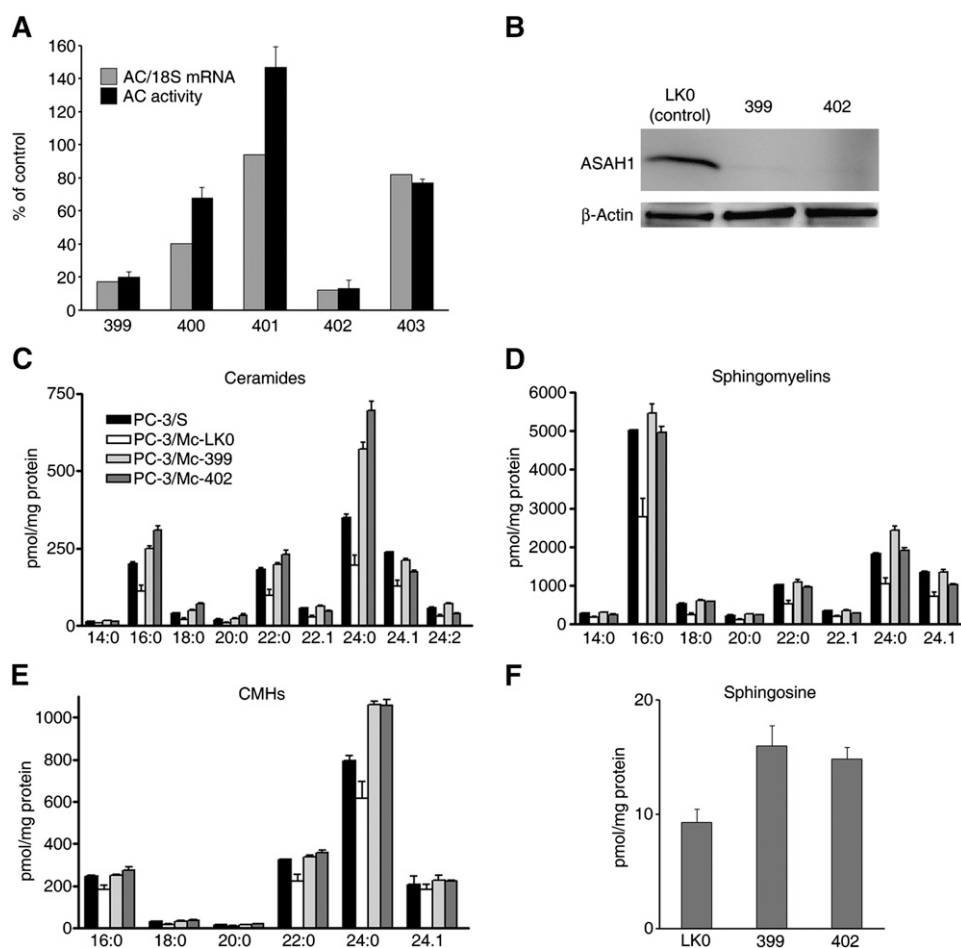


**Fig. 2.** ASAHI knockdown causes an accumulation of sphingolipids in PC-3/Mc cells. A: Knockdown of *ASAHI* mRNA by five distinct shRNAs, determined by qPCR, and of AC activity as determined with RBM14C12 as a substrate in intact cells. Negative controls were PC-3/Mc cells transduced with lentiviral particles carrying a LK0 vector expressing a nontargeting shRNA sequence. Results were normalized to 18S mRNA or amount of protein. Values are represented as the mean percentage over control of three replicates  $\pm$  SD. B: Western blotting confirmatory of the specific and effective knockdown of ASAHI mRNA by shRNAs 399 and 402. Actin signal was used as a control of protein loading and transfer. C–F: Sphingolipid content of PC-3/Mc cells knocked down for ASAHI with shRNAs 399 and 402, showing the accumulation of ceramides (C), sphingomyelins (D), ceramide monohexosides (E), and sphingosine (F) compared with control PC-3/Mc-LK0 cells. Determinations were carried out by UPLC/TOF. Results are shown as the mean of three values  $\pm$  SD.

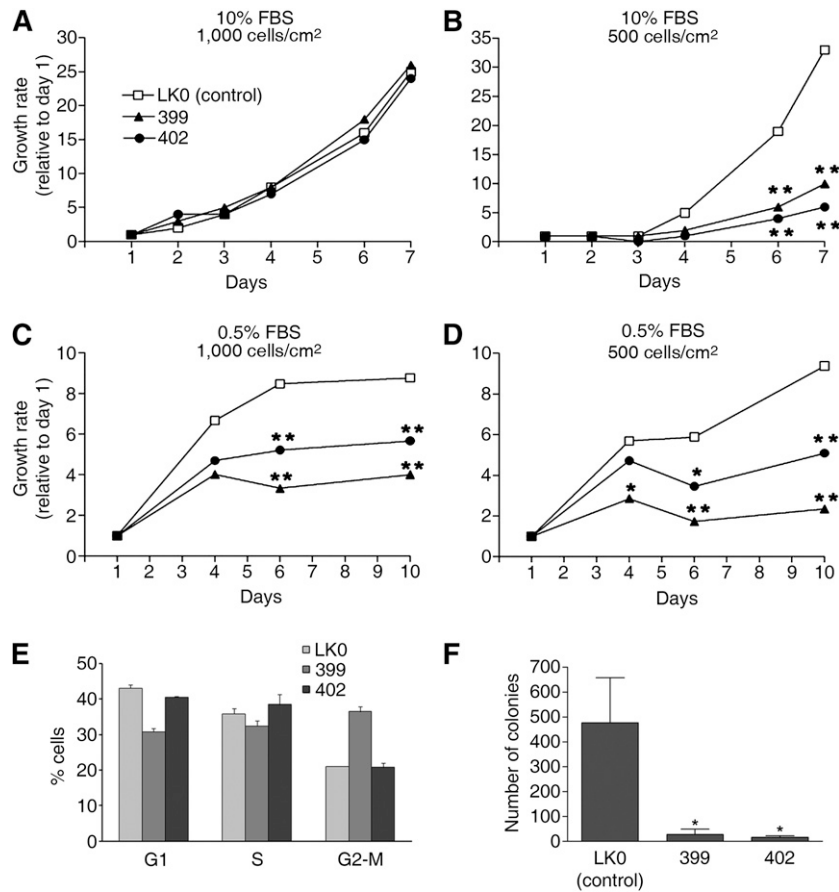


**Fig. 3.** ASAHI knockdown inhibits the growth of PC-3/Mc cells under low-density and low-serum conditions and abrogates their anchorage-independent colony-forming potential. A–D: Effect of ASAHI knockdown by shRNA 399 or 402 on the 2D growth of PC-3/Mc cells. Cells were seeded at the specified initial densities on plastic dishes and grown in medium supplemented with either 10% FBS (A, B) or 0.5% FBS (C, D). Controls were PC-3/Mc cells transduced with lentiviral particles carrying a LK0 vector expressing a nontargeting shRNA sequence. The number of cells was determined with the MTT method at the indicated time points after seeding. Data correspond to the mean  $\pm$  SD of triplicates. Statistical significance: \* $P < 0.05$ , \*\* $P < 0.005$  (two-tailed unpaired *t*-test). E: Effect of ASAHI knockdown on the cell cycle distribution of PC-3/Mc cells. Cells stably transduced with the indicated lentiviral particles or a control vector (LK0) were analyzed for DNA content by flow cytometry and analyzed for cell cycle distribution. Data are represented as the mean of triplicates  $\pm$  SD. F: Effect of ASAHI knockdown by shRNA 399 or 402 on anchorage-independent cell growth of PC-3/Mc cells. Cells were cultured on soft agar, and colonies were stained with crystal violet after three weeks. Data are represented as the mean of triplicates  $\pm$  SD.

than control cells at all initial seeding densities, with more pronounced effects at the lowest initial seeding density studied (Fig. 3C, D).

In agreement with the weak effect of ASAHI knockdown on the growth of PC-3/Mc cells in standard culture conditions, only one of the two ASAHI-specific shRNAs caused a modest decline of the G1 population with an increased G2-M population (Fig. 3E). The ability of cells to form colonies in anchorage-independent conditions is a measure of their self-renewal potential and is closely related to their tumorigenic and metastatic capacities in vivo (25). As described above, the metastatic PC3/Mc cells were strongly clonogenic, as opposed to the nonmetastatic PC-3/S cells. Knockdown of ASAHI completely abolished the clonogenic capacity of PC-3/Mc cells (Fig. 3F), indicating that ASAHI is required for their self-renewal. Consistently, knockdown of ASAHI strongly inhibited the ability of

PC-3/Mc cells to form tumors in NOD-SCID mice, with independence of the initial inoculum size (Fig. 4A), and it significantly delayed their ability to colonize lungs upon intravenous injection (Fig. 4B).

Therefore, although PC-3/Mc cells are resistant to the effects on survival or the cell cycle caused by ceramide accumulation following knockdown of ASAHI, they display a strong dependence on ASAHI for the maintenance of key properties associated with tumor-initiating cells, namely, anchorage-independent growth in vitro and tumorigenesis and lung colony formation in immunodeficient mice.

#### Development of novel, highly specific acid ceramidase inhibitors

The above results support the importance of ASAHI for the self-renewal and metastatic phenotypes of PC-3 prostate cancer cells, and validate it as a potential therapeutic

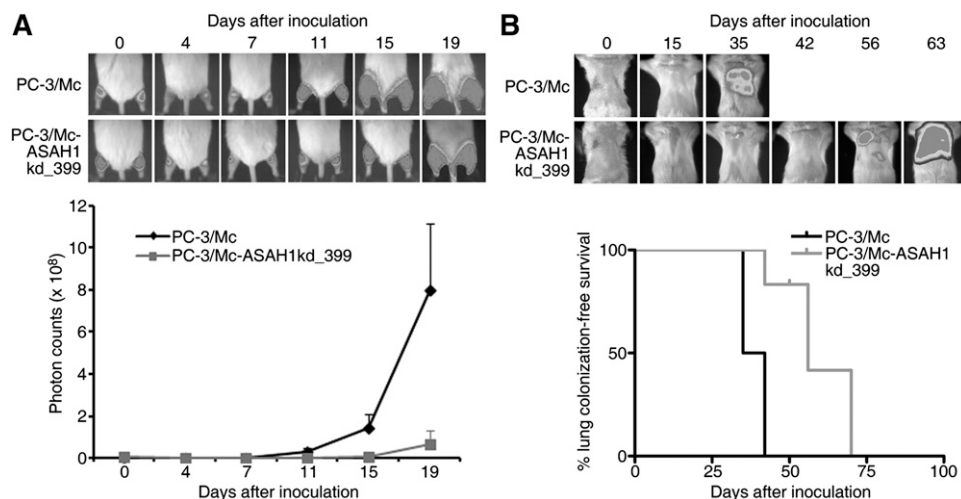


**Fig. 4.** ASAHI knockdown inhibits tumor growth and lung colonization of PC-3/Mc cells in NOD-SCID mice. **A:** Knock down of ASAHI in PC-3/Mc cells with shRNA 399 strongly inhibits the growth of tumors. Controls were PC-3/Mc cells transduced with lentiviral particles carrying a LK0 vector expressing a nontargeting shRNA. Cells ( $2 \times 10^5$ ) were inoculated intramuscularly in male NOD-SCID mice, and growth was monitored by bioluminescence. Upper panel: bioluminescent images of representative mice. Lower panel: Growth curves as a function of time ( $n = 8$ ). **B:** Knockdown of ASAHI in PC-3/Mc cells with shRNA 399 significantly delays lung colonization. Control cells were as in (A). Cells ( $2 \times 10^5$ ) were inoculated intravenously in male NOD-SCID mice, and lung colonization was monitored by bioluminescence. Upper panel: bioluminescent images of representative mice. Lower panel: Kaplan-Maier plots of lung colonization free-mice as a function of time ( $n = 8$ ).

target in hormone-insensitive, metastatic prostate cancer. Several AC inhibitors have been synthesized and tested with potencies in the low micromolar range. Considering that AC is a cysteine hydrolase, a small family of ceramide analogs modified at the amide linkage with thiol reactive functions was generated and tested. These compounds were inspired in reported cysteine protease inhibitors (26) and include two  $\alpha$ -haloamides and several  $\alpha,\beta$ -unsaturated amides as Michael acceptors. Their structures are shown in **Fig. 5A**.

The RBM1 series of compounds was synthesized by *N*-acylation of dihydrosphingosine following standard procedures. All compounds were tested in intact FD10X cells as well as in cell lysates at pH 4.5 following the reported fluorogenic assay (22, 27). The best inhibitors in intact cells were compounds RBM1-12, RBM1-13, RBM1-18, and SABRAC, with percentages of inhibition ranging from 50 to 70% (**Fig. 5B**). Whereas RBM1-12, RBM1-13, and SABRAC maintained their inhibitory activities in the *in vitro* assay, RBM1-18 had no inhibitory activity in cell lysates (**Fig. 5B**). Therefore, compounds RBM1-12, RBM1-13, and SABRAC were selected for further studies. To assess their specificity, the three compounds were tested for their effects on NC using the standard substrate (28) and on FD cells transiently transfected with the ASAHI2 gene. None of the compounds inhibited NC (**Fig. 5C**), attesting to their specificity as inhibitors of acid ceramidase. *In vitro* dose-response determinations showed that SABRAC was the best inhibitor, with an  $IC_{50}$  value of 52 nM, followed by RBM1-12 ( $IC_{50} = 0.53 \mu\text{M}$ ) and RBM1-13, which exhibited the lowest potency ( $IC_{50} = 11.2 \mu\text{M}$ ) (**Fig. 5D**). Furthermore, both in the presence of SABRAC or RBM1-12, the enzyme activity

experienced an exponential decay versus incubation time at the two protein concentrations tested (supplementary **Fig. 1**), indicating an irreversible type of inhibition.

Neither SABRAC nor RBM1-12 inhibited the activity of the cysteine protease papain, whereas chymostatin completely blocked papain activity at the standard concentrations (supplementary **Fig. IIA**). On the other hand, at conditions under which SABRAC inhibited AC, AC activity was unaffected by the cysteine protease inhibitor E64d (supplementary **Fig. IIB**).

#### Effects of AC inhibitors on the growth of PC-3/Mc cells

We next tested the effects of RBM1-12, RBM1-13, and SABRAC on the growth properties of PC-3/Mc cells. First, the inhibitory potency of these compounds on AC was determined by incubating the cells with increasing doses for 48 h, and then determining AC activity in cell lysates using a fluorogenic assay. Under these conditions, the inhibition of AC by RBM1-12 and SABRAC was dose-dependent (RBM1-12:  $1 \mu\text{M} < IC_{50} < 5 \mu\text{M}$ ; SABRAC:  $IC_{50} < 1 \mu\text{M}$ ) (**Fig. 6A**). Surprisingly, RBM1-13, which had shown to be a good AC inhibitor in FD10X intact cells and cell lysates (**Fig. 5B**), did not display any AC inhibitory effect in PC-3/Mc cells. In fact, RBM1-13 tended to enhance the activity of AC in these cells (**Fig. 6A**). We do not know the reason for this striking difference in the effects of RBM1-13 between these two cell lines, although differential metabolism or uptake of the compounds in the prostate cancer cell lines tested may contribute to the discrepancy. The sphingolipid profiles of PC-3/Mc cells after treatment with these compounds reflected their AC inhibitory activities. Thus, both RBM1-12 and SABRAC induced an accumulation



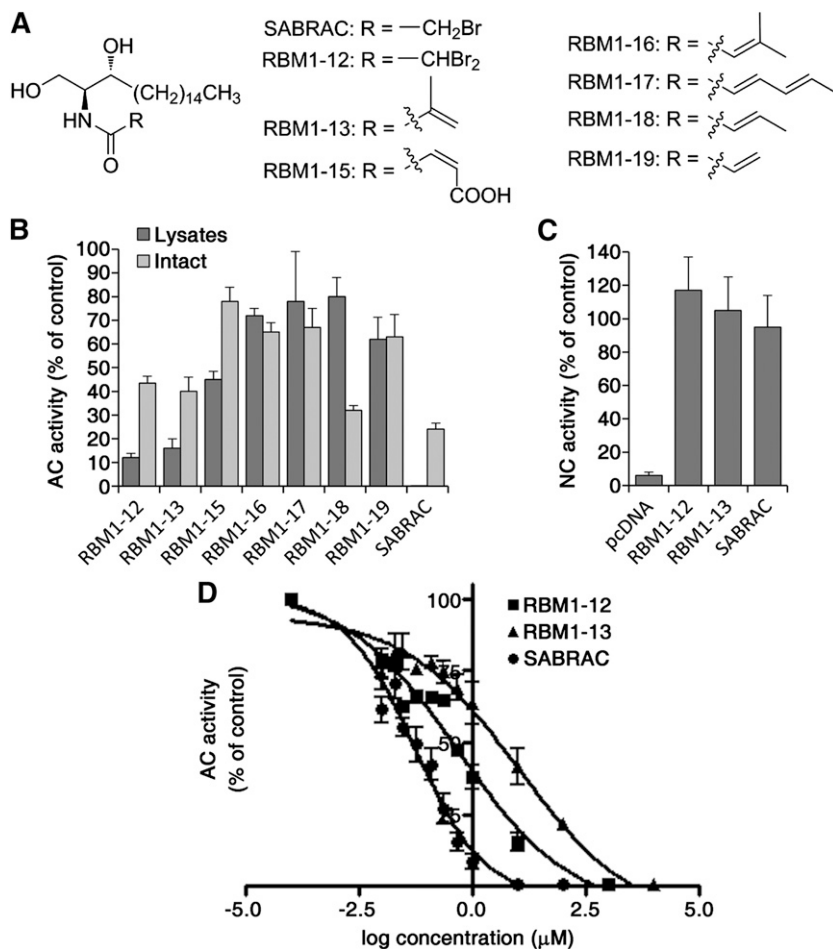


**Fig. 5.** Novel acid ceramidase inhibitors: structures and activities. A: Chemical structure of the compounds. B: AC activities as determined in FD10X cells with equimolar concentrations (40  $\mu\text{M}$ ) of substrate (RBM14C12) and test compound. Control activities correspond to those of FD10X. C: NC activities as measured in FD cells transfected with pcDNA5/TO\_ASAH2 using CerC12NBD as substrate (5  $\mu\text{M}$ ) and test compounds at 40  $\mu\text{M}$  or vehicle (control). D: Dose-response AC activities of selected compounds on FD10X cell lysates assayed with RBM14C12 for 3 h after 5 min incubation with different concentrations of RBM1-12, RBM1-13, and SABRAC. Data points correspond to the mean  $\pm$  SD of two experiments with triplicates. In all cases, results were normalized to the amount of protein (in vitro) or number of cells (intact), which was similar in all cases. Controls were as in (B). Regression analysis of data in (D) (sigmoidal dose-response with variable slope) affords  $\text{IC}_{50}$  values of 0.53  $\mu\text{M}$ , 11.2  $\mu\text{M}$ , and 52 nM for RBM1-12, RBM1-13, and SABRAC, respectively.

of ceramides (Fig. 6B), whereas, as expected for its lack of AC inhibitory activity in PC-3/Mc cells, RBM1-13 did not significantly alter the abundance of ceramides.

The abundance of complex sphingolipids such as SM or CMH was not significantly affected by any of the compounds, except for the levels of CMH in cells treated with RBM1-12 at 5  $\mu\text{M}$ , which increased 50% over controls (Fig. 6B). This is in contrast with the effect of stably knocking down ASAHI in PC-3/Mc cells, which caused the accumulation of these complex sphingolipids (Fig. 2D, E). In a second discrepancy between transcript knockdown and chemical inhibition of AC, levels of sphingosine did not change by treatment of PC-3/Mc cells with either RBM1-12 or SABRAC (data not shown), whereas they increased upon ASAHI knockdown. We speculate that prolonged knockdown of ASAHI may permit an adaptive response of cells by upregulating other ceramides to

facilitate the removal of the ceramides that accumulate as a consequence of ASAHI silencing. The short-term inhibition of AC by chemical inhibitors, such as in the above experiments, would not allow sufficient time to trigger such hypothetical long-term adaptive responses.

These compounds were assessed for their effects on the growth of PC-3/Mc cells. At a concentration of 5  $\mu\text{M}$  and in medium containing 10% FBS, the growth of PC-3/Mc cells was significantly slowed by all the compounds, although RBM1-13 showed the least growth inhibitory activity at 1  $\mu\text{M}$  (Fig. 6C). At 5  $\mu\text{M}$ , the two AC inhibitors active on PC-3/Mc cells, RBM1-12 and SABRAC, completely abolished the ability of PC-3/Mc cells to form colonies in anchorage-independent conditions, while RBM1-13 did not show significant effects in these assays (Fig. 6D). None of the compounds had significant effects at a concentration of 1  $\mu\text{M}$ , and similar to knockdown of ASAHI, none

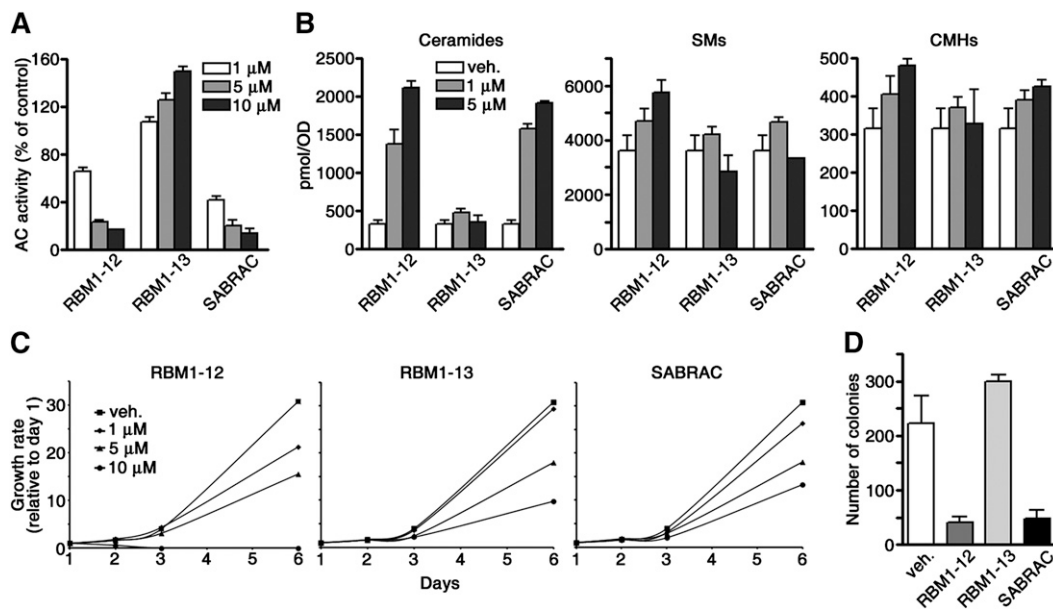


**Fig. 6.** Effects of novel ceramidase inhibitors on the AC activity and growth of PC-3/Mc cells. **A:** AC activity of PC3/Mc cells treated with RBM1-12, RBM1-13, or SABRAC. Cells were treated with the compounds at the specified concentrations for 48 h, and AC activity was determined in cell lysates with RBM14C12 as the substrate (40 μM). Results, normalized for protein quantity, are shown as the mean of three values ± SD. **B:** Sphingolipid content of PC3/Mc cells treated with 1 or 5 μM RBM1-12, RBM1-13, or SABRAC for 48 h. Results were normalized for protein quantity and shown as mean of triplicates ± SD. **C:** Effect of RBM1-12, RBM1-13, and SABRAC on the adherent growth of PC-3/Mc cells under standard culture conditions. Cells (1,000/cm<sup>2</sup>) were seeded in 96-well plates, and cell numbers were determined with the MTT method at different time points. Data are represented as the mean of triplicates ± SD. **D:** Effect of RBM1-12, RBM1-13, and SABRAC on the anchorage-independent growth of PC-3/Mc cells. Cells (3 × 10<sup>3</sup>) were cultured in soft agar in the presence of 5 μM of the test compounds or vehicle alone, and then stained with crystal violet after three weeks. Images were captured and processed with ImageJ, and colonies ≥ 0.2 mm diameter were scored. Data are represented as the mean of triplicates ± SD.

of the inhibitors caused significant changes in the cell cycle profile of PC-3/Mc cells (data not shown).

Next, the dose-dependent cytotoxic activity of these compounds on PC-3/Mc cells was evaluated after 72 h incubations. The most toxic compound was RBM1-13 (CC<sub>50</sub> = 10.0 μM), followed by RBM1-12 (CC<sub>50</sub> = 28.2 μM) and SABRAC (CC<sub>50</sub> > 300 μM) (supplementary Fig. III). Because RBM1-13 did not show a detectable AC inhibitory activity in PC-3/Mc cells, its cytotoxic activity on these cells must be caused by off-target effects. The non-metastatic PC-3/S clone was more sensitive to the cytotoxic effects of SABRAC than were the isogenic, metastatic PC-3/Mc cells, (CC<sub>50</sub> = 25.3 μM). In contrast, both clones exhibited similar sensitivities to RBM1-12 and RBM1-13 (CC<sub>50</sub> = 37.4 μM and 14.6 μM, respectively) (supplementary Fig. III). The cytotoxic activity of these compounds was tested on additional pairs of cell lines with different tumorigenic or metastatic potentials, including the transformed prostate epithelial cells RWPE-2 (tumorigenic) versus RWPE-1 (nontumorigenic), the lung cancer cell lines HAL8 (metastatic) versus HAL24 (nonmetastatic), and the breast cancer cell lines MDA-MB-231 (metastatic) versus MCF-7 (nonmetastatic). The less aggressive cell lines were generally more sensitive to the cytotoxic activity of these acid ceramidase inhibitors than were their more aggressive partners (supplementary Fig. III).

In summary, similar to ASAHI knockdown, two of the newly developed AC inhibitors, RBM1-12 and SABRAC, showed strong inhibitory activities on AC activity and on the growth and clonogenic capacities of the highly metastatic PC-3/Mc cells. Interestingly, SABRAC displayed strong growth inhibitory effects on PC-3/Mc cells, while exhibiting very limited cytotoxicity. A third compound, RBM1-13, which had AC inhibitory activity in other cells, did not inhibit AC in PC-3/Mc cells, and although it exerted cytotoxic activity on these cells, it had less potent inhibitory activity on the growth of these cells on plastic and showed no effect on their capacity to grow in anchorage-independent conditions.

#### Expression of ASAHI in nonmetastatic and metastatic prostate cancer

It has previously been reported that ASAHI is expressed in a number of tumor types, including PC, at levels higher than in normal tissues (17). However, thus far its expression in PC has not been reported by immunohistochemistry, which permits to correlate staining intensities (as surrogates of expression levels) with morphological parameters. We used an ASAHI-specific antibody (Figs. 1H and 2B) to analyze by immunohistochemistry a total of 33 samples from prostate cancer patients that contained tumoral glands, glands with normal morphologies, and

glands with characteristics of the preneoplastic lesion prostate intraepithelial neoplasia (PIN). All epithelial structures stained for ASAHI, albeit at varying intensities (Fig. 7A–C). In a range of staining intensities from 1 to 3, most normal or neoplastic structures were given an intensity score of 2 (72.7% of normal glands, 75% of PIN, and 63.6% of tumoral glands; Fig. 7D and supplementary Table I). However, only 1 out of 22 evaluable cases with normal glands was scored as intensity 3 (4.5%), while 4 of 24 (16.7%) of PIN glands and 10 of 33 (30.3%) of tumoral glands were scored as intensity 3 (Fig. 7D and supplementary Table II). In those cases in which normal and tumoral glands could be evaluated simultaneously in the same sample (22 cases), the ASAHI staining intensities of normal versus tumoral glands were scored as equal in 10 cases (45.5%), the staining intensity was scored as stronger in tumoral glands versus normal glands in 8 cases (36.4%), and in 4 cases (18.2%), the maximum intensity in tumoral glands was scored as lower than the maximum intensity in normal glands (Fig. 7E and supplementary Table II). In several cases, the staining intensity for ASAHI in tumoral areas was clearly stronger than the staining in adjacent normal glands (Fig. 7C, E).

Thus, strong ASAHI immunostaining in human prostate tissues tended to be associated with prostate adenocarcinoma (Fig. 7D), an observation that complements previous reports in which immunohistochemical analysis was not performed, and thus the specific cell type, either epithelial or stromal, expressing ASAHI was not determined (17). On the other hand, with the cases studied here, stronger ASAHI staining did not show correlations

with histological grade (Gleason score), stage, or the presence of lymph node metastasis. However, the observation that strong expression of ASAHI was associated with the preneoplastic PIN lesions more than with normal glands and in turn with prostate adenocarcinoma more than with PIN lesions suggests that ASAHI expression levels tend to increase during PC progression.

## DISCUSSION

Advanced, hormone-independent, castration-resistant prostate cancer represents a devastating form of the disease that frequently develops from initially less aggressive tumors and shows resistance to conventional chemotherapeutic agents (18–20). In this evolutive process, the progressive dominance in the tumor of cancer stem cells, endowed with high survival and low drug sensitivity (25, 29), is emerging as crucial.

Here, we studied the clonal population PC-3/Mc, derived from prostate cancer cells and highly enriched in tumor-initiating cells (21), and found that its growth and clonogenic potential are extremely sensitive to the knockdown of ASAHI or chemical inhibition of AC activity. In addition, knockdown of ASAHI in these cells strongly inhibited their capacity to grow tumors upon local implantation or to colonize lungs after intravenous injection. Although the growth of PC-3/Mc cells under adherent conditions was also affected by ASAHI knockdown, it was made most evident only upon deprivation of growth factors, suggesting that ASAHI is required for optimal

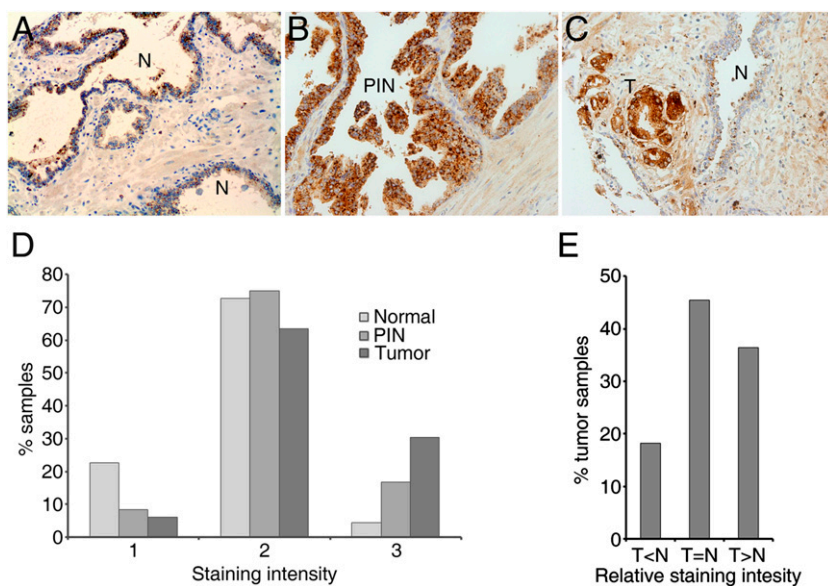


**Fig. 7.** Immunohistochemical analysis of ASAHI expression in prostate cancer. A–C: Staining for ASAHI with a specific antibody of 33 cases of prostate cancer showed expression in normal glands (A), glands with prostate intraepithelial neoplasia or PIN (B), and adenocarcinomatous glands (C), with frequent (36.4% of cases) stronger staining in tumoral (T) than in morphologically normal (N) glands. D: Stronger staining (intensity 3) was observed more frequently in adenocarcinomatous glands (Tumor) than in PIN and morphologically normal glands. E: In samples in which tumoral and morphologically normal glands were analyzed simultaneously, the staining intensities were scored as equal in tumoral versus normal glands in 45.5%, as stronger in tumoral versus normal glands in 36.4%, and as weaker in tumoral versus normal glands in 18.2% of cases.

growth of PC-3/Mc cells under limited growth factor supply but is dispensable for adherent growth when growth factors are present at high concentrations. These results, together with the strong phenotype that we observed in anchorage-independent growth assays, which correlates with self-renewal, tumorigenic, and metastatic potentials (21, 25) for both ASAH1 knockdown and AC inhibition, suggest that AC is required for self-renewal and growth factor signaling in drug-resistant and metastatic PC-3/Mc prostate cancer cells.

That ASAH1 knockdown and inhibition of AC produces a specific effect on a particular growth property of PC-3/Mc cells, namely, anchorage-independent spheroid formation, is further supported by the absence of significant cell death or the accumulation of sub-G1 cell populations, in spite of the expected accumulation of ceramides. Additionally, neither ASAH1 knockdown nor AC inhibition caused a significant sensitization of PC-3/Mc cells to drugs used in advanced prostate cancer therapy, including docetaxel, doxorubicin, and etoposide (supplementary Fig. IV), which confirms the chemoresistance of this highly aggressive subpopulation of prostate cancer cells enriched in tumor-initiating cells unaffected by the accumulation of ceramides. The failure of AC inhibition or ASAH1 knockdown to chemosensitize PC-3/Mc cells differs from the sensitization found in various other tumor cells (30–39). In PC-3/Mc cells, AC inhibition or ASAH1 knockdown may upregulate specific pathways to metabolize the resulting ceramide excess. Such pathways include phosphorylation, glycosylation, and conversion into SM. The possibility of phosphorylation as a tumor death escape route (40) does not seem plausible, as no ceramide-1-phosphate was ever detected in PC-3/Mc cells, regardless of any genetic manipulation or chemical treatment. In contrast, most SM and CMH species are significantly higher in ASAH1-knockdown cells than in mock cells. Although SM synthases have been seldom addressed as targets to overcome resistance (41, 42), the usefulness of inhibition of glucosyltransferases as a means to exploit ceramide as an antitumor agent has been extensively documented (43, 44). Furthermore, chemoresistance is not only the result of ceramide clearance by glycosylation but also the increased glycosylation products themselves have been reported to upregulate the expression of multidrug resistant protein 1 (MDR1) through c-Src kinase and  $\beta$ -catenin signaling (45). Whether UDP-glucose ceramide glucosyltransferase (UGCG) or MDR1 is upregulated upon ASAH1 silencing in PC-3/Mc cells has not been investigated. However, the UGCG transcript levels are higher in PC-3/S than in PC-3/Mc cells (unpublished observations), as opposed to their AC activity.


Nevertheless, the significant increase in SM and CMH in PC-3/Mc cells knocked down for AC deserves comment. Because AC is a lysosomal enzyme and ceramides cannot exit from the lysosome (46), a lack of AC activity leads to an intralysosomal accumulation of ceramide. However, sphingomyelin synthase 2 is localized in the plasma membrane, whereas sphingomyelin synthase 1 and glucosylceramide synthase reside in the Golgi apparatus (14, 47).

Because of this different enzyme compartmentalization, the increase in SM and CMH is unlikely to arise from augmented synthesis from the lysosomal ceramide. A plausible explanation involves downregulation of lysosomal acid sphingomyelinase and glucocerebrosidase as a result of intralysosomal ceramide buildup. Interestingly, the sphingolipid profile of the PC-3/Mc cells knocked down for AC is similar to that seen in PC-3/S cells. This finding supports that the accumulation of sphingolipids inside the lysosome as a result of different AC activities in both clones is related to the different aggressiveness of the two phenotypes.

The growing recognition of AC as a potential therapeutic target in cancer has encouraged the development of AC inhibitors (12). AC belongs to the *N*-terminal nucleophile (Ntn) hydrolase family (48). This family of enzymes shares the common feature of having an *N*-terminal nucleophile, which is generated by autoproteolytic processing (49). The Cys143 nucleophilic thiol in AC is exposed at the *N*-terminus of the  $\beta$ -subunit after cleavage of the precursor protein. Therefore, AC belongs to the same subcategory of Ntn hydrolases as the cysteine proteases. Based on this relationship, AC has been recently found to be inhibited by the cysteine protease inhibitors, cystatins (50). During the course of this study, we identified novel potent and specific inhibitors of AC within a series of small molecules inspired in reported irreversible cysteine protease inhibitors (51–53). These compounds feature either an  $\alpha$ -halocarbonyl unit or an  $\alpha,\beta$ -double-bond Michael acceptor moiety. The first screening in cells overexpressing AC showed that, among the compounds prepared, the  $\alpha$ -bromoamides RBM1-12 and SABRAC were the most potent inhibitors. Within the  $\alpha,\beta$ -unsaturated amides, only the methacrylamide (RBM1-13) elicited AC inhibitory activities both in intact cells and cell lysates. None of the compounds was active on NC, consistent with their conception as thiol-targeting molecules. The low potencies of the other  $\alpha,\beta$ -unsaturated amides relative to RBM1-13 suggest that substitution at the  $\beta$ -position hinders the attack of the enzyme nucleophilic thiolate. Surprisingly, acrylamide RBM1-19 had no activity as AC inhibitor. Although the reasons for this finding have not been investigated, it is possible that the high reactivity of unsubstituted acrylamides results in alternative reactions of RBM1-19 before reaching the AC target. The activity of the bromoamides is especially relevant. SABRAC and RBM1-12 are among the most potent AC inhibitors so far reported (54), with  $IC_{50}$  values of 52 nM and 530 nM, respectively, as assayed with lysates of cells overexpressing AC. Time dependence of inhibition supported that both SABRAC and RBM1-12 are irreversible inhibitors, which agrees with the expected mechanism considering their structure and the involvement of a nucleophilic cysteine residue in the catalytic site. Furthermore, they are inactive over both NC and papain, a cysteine protease, thus supporting their selectivity for AC.

Both SABRAC and RBM1-12 were also potent inhibitors of AC in intact PC-3/Mc cells. Surprisingly, RBM1-13, which inhibited AC in FD10X cells, failed to inhibit AC in

the PC-3/Mc cell line. This difference is likely due to the different incubation times (FD10X, 4 h; PC3Mc, 48 h) pointing to the metabolization of RBM1-13 after long-term incubations. In contrast, the bromoamides maintained their inhibitory activity at long incubation times. In agreement with their AC inhibitory activity, both SABRAC and RBM1-12 induced a buildup of ceramides, which was significant compared with controls for all the different *N*-acyl species. However, levels of sphingosine remained unaffected. The latter results, although unexpected for AC inhibitors, are not unprecedented. Bielawska et al. (55) reported that the sphingolipid profiles of MCF-7 cells treated with different ceramidase inhibitors derived from B13 and D-e-MAPP followed different patterns depending on the chemical function substituted for the original amide. In the case of an *N*-alkyl analog of D-e-MAPP, namely, compound LCL284, ceramides accumulated, but long chain bases did not change significantly. A plausible explanation is the triggering of compensatory mechanisms to keep bioactive sphingolipids at nonlethal levels. One such mechanism could involve an increased activity of other ceramidases. A similar scenario might lead to the slight increase of sphingosine found in PC-3/Mc cells knocked down for AC. In support of this hypothesis, Hu et al. (24) demonstrated that knockdown of the alkaline ceramidase 3 upregulated the expression of the alkaline ceramidase 2 with increases of both sphingosine and its phosphate.

Our findings support the notion that ceramidase metabolism (56) and, more specifically, acid ceramidase activity, are critical regulators of the self-renewal, tumorigenic, and metastatic potentials of cancer stem cells, represented by the PC-3/Mc population (21), beyond their known regulation of signals that tilt the balance between cell survival and death. Furthermore, we argue that our cellular model, specifically selected for subpopulations with strong self-renewal and aggressive phenotypes, allows to better address therapeutic strategies against advanced cancer (45). The precise mechanism linking the elevated AC activity and the increased aggressiveness of PC-3/Mc cells compared with the PC-3/S clone is under investigation. 

The authors thank Mònica Marín and Laura Gelabert (Tumor Bank, Biobank) for tissue processing and immunohistochemistry, Jaume Comas (Barcelona Science Park core facilities) for assistance with flow cytometry, and Artur Sixto (Office for Technology Transfer, CSIC) for catalyzing this collaboration and providing critical assistance with intellectual property issues.

## REFERENCES

- Hirsch, H. A., D. Iliopoulos, A. Joshi, Y. Zhang, S. A. Jaeger, M. Bulyk, P. N. Tschlis, X. Shirley Liu, and K. Struhl. 2010. A transcriptional signature and common gene networks link cancer with lipid metabolism and diverse human diseases. *Cancer Cell*. **17**: 348–361.
- Menendez, J. A., and R. Lupu. 2007. Fatty acid synthase and the lipogenic phenotype in cancer pathogenesis. *Nat. Rev. Cancer*. **7**: 763–777.
- Mashima, T., H. Seimiya, and T. Tsuruo. 2009. De novo fatty-acid synthesis and related pathways as molecular targets for cancer therapy. *Br. J. Cancer*. **100**: 1369–1372.
- Kourtidis, A., R. Srinivasaiah, R. D. Carkner, M. J. Brosnan, and D. S. Conklin. 2009. Peroxisome proliferator-activated receptor-gamma protects ERBB2-positive breast cancer cells from palmitate toxicity. *Breast Cancer Res.* **11**: R16.
- Delgado, A., J. Casas, A. Llebaria, J. L. Abad, and G. Fabrias. 2006. Inhibitors of sphingolipid metabolism enzymes. *Biochim. Biophys. Acta*. **1758**: 1957–1977.
- Kolesnick, R. N., and M. Kronke. 1998. Regulation of ceramide production and apoptosis. *Annu. Rev. Physiol.* **60**: 643–665.
- Hannun, Y. A., and L. M. Obeid. 1995. Ceramide: an intracellular signal for apoptosis. *Trends Biochem. Sci.* **20**: 73–77.
- Ogretmen, B., and Y. A. Hannun. 2004. Biologically active sphingolipids in cancer pathogenesis and treatment. *Nat. Rev. Cancer*. **4**: 604–616.
- Liu, X., S. Elojeimy, L. S. Turner, A. E. Mahdy, Y. H. Zeidan, A. Bielawska, J. Bielawski, J. Y. Dong, A. M. El-Zawahry, G. W. Guo, et al. 2008. Acid ceramidase inhibition: a novel target for cancer therapy. *Front. Biosci.* **13**: 2293–2298.
- Henry, B., C. Moller, M. T. Dimanche-Boitrel, E. Gulbins, and K. A. Becker. Targeting the ceramide system in cancer. *Cancer Lett.* Epub ahead of print. July 23, 2011; doi:10.1016/j.canlet.2011.07.010.
- Bornancin, F. 2011. Ceramide kinase: the first decade. *Cell. Signal.* **23**: 999–1008.
- Gangoiti, P., L. Camacho, L. Arana, A. Ouro, M. H. Granado, L. Brizuela, J. Casas, G. Fabrias, J. L. Abad, A. Delgado, et al. 2010. Control of metabolism and signaling of simple bioactive sphingolipids: implications in disease. *Prog. Lipid Res.* **49**: 316–334.
- Pitson, S. M. 2011. Regulation of sphingosine kinase and sphingolipid signaling. *Trends Biochem. Sci.* **36**: 97–107.
- Holthuis, J. C., and C. Luberto. 2010. Tales and mysteries of the enigmatic sphingomyelin synthase family. *Adv. Exp. Med. Biol.* **688**: 72–85.
- Wennekes, T., R. J. Berg, R. G. Boot, G. A. van der Marel, H. S. Overkleeft, and J. M. Aerts. 2009. Glycosphingolipids—nature, function, and pharmacological modulation. *Angew. Chem. Int. Ed. Engl.* **48**: 8848–8869.
- Norris, J. S., A. Bielawska, T. Day, A. El-Zawahry, S. Elojeimy, Y. Hannun, D. Holman, M. Hyer, C. Landon, S. Lowe, et al. 2006. Combined therapeutic use of AdGFP FasL and small molecule inhibitors of ceramide metabolism in prostate and head and neck cancers: a status report. *Cancer Gene Ther.* **13**: 1045–1051.
- Seelan, R. S., C. Qian, A. Yokomizo, D. G. Bostwick, D. I. Smith, and W. Liu. 2000. Human acid ceramidase is overexpressed but not mutated in prostate cancer. *Genes Chromosomes Cancer*. **29**: 137–146.
- Ferlay, J., D. M. Parkin, and E. Steliarova-Foucher. 2010. Estimates of cancer incidence and mortality in Europe in 2008. *Eur. J. Cancer*. **46**: 765–781.
- Pienta, K. J., and D. Bradley. 2006. Mechanisms underlying the development of androgen-independent prostate cancer. *Clin. Cancer Res.* **12**: 1665–1671.
- Yap, T. A., A. Zivi, A. Omlin, and J. S. de Bono. 2011. The changing therapeutic landscape of castration-resistant prostate cancer. *Nat. Rev. Clin. Oncol.* **8**: 597–610.
- Celià-Terrassa, T., O. Meca-Cortes, F. Mateo, A. M. de Paz, N. Rubio, A. Arnal-Estape, B. J. Ell, R. Bermudo, A. Diaz, M. Guerra-Rebollo, et al. 2012. Epithelial-mesenchymal transition can suppress major attributes of human epithelial tumor-initiating cells. *J. Clin. Invest.* **122**: 1849–1868.
- Bedia, C., L. Camacho, J. L. Abad, G. Fabrias, and T. Levade. 2010. A simple fluorogenic method for determination of acid ceramidase activity and diagnosis of Farber disease. *J. Lipid Res.* **51**: 3542–3547.
- Filippova, I. Yu, E. N. Lysogorskaya, E. S. Oksenoit, G. N. Rudenskaya, and V. M. Stepanov. 1984. L-Pyroglutamyl-L-phenylalanyl-L-leucine-p-nitroanilide—a chromogenic substrate for thiol proteinase assay. *Anal. Biochem.* **143**: 293–297.
- Hu, W., R. Xu, W. Sun, Z. M. Szulc, J. Bielawski, L. M. Obeid, and C. Mao. 2010. Alkaline ceramidase 3 (ACER3) hydrolyzes unsaturated long-chain ceramides, and its down-regulation inhibits both cell proliferation and apoptosis. *J. Biol. Chem.* **285**: 7964–7976.
- Visvader, J. E., and G. J. Lindeman. 2008. Cancer stem cells in solid tumours: accumulating evidence and unresolved questions. *Nat. Rev. Cancer*. **8**: 755–768.
- Otto, H. H., and T. Schirmeister. 1997. Cysteine proteases and their inhibitors. *Chem. Rev.* **97**: 133–172.

27. Bedia, C., J. Casas, V. Garcia, T. Levade, and G. Fabrias. 2007. Synthesis of a novel ceramide analogue and its use in a high-throughput fluorogenic assay for ceramidases. *ChemBioChem*. **8**: 642–648.
28. Tani, M., N. Okino, S. Mitsutake, and M. Ito. 1999. Specific and sensitive assay for alkaline and neutral ceramidases involving C12-NBD-ceramide. *J. Biochem.* **125**: 746–749.
29. Ben-Porath, I., M. W. Thomson, V. J. Carey, R. Ge, G. W. Bell, A. Regev, and R. A. Weinberg. 2008. An embryonic stem cell-like gene expression signature in poorly differentiated aggressive human tumors. *Nat. Genet.* **40**: 499–507.
30. Bai, A., Z. M. Szulc, J. Bielawski, N. Mayroo, X. Liu, J. Norris, Y. A. Hannun, and A. Bielawska. 2009. Synthesis and bioevaluation of omega-N-amino analogs of B13. *Bioorg. Med. Chem.* **17**: 1840–1848.
31. Bedia, C., J. Casas, N. Andrieu-Abadie, G. Fabrias, and T. Levade. 2011. Acid ceramidase expression modulates the sensitivity of A375 melanoma cells to dacarbazine. *J. Biol. Chem.* **286**: 28200–28209.
32. Canals, D., D. M. Perry, R. W. Jenkins, and Y. A. Hannun. 2011. Drug targeting of sphingolipid metabolism: sphingomyelinases and ceramidases. *Br. J. Pharmacol.* **163**: 694–712.
33. Elojeimy, S., X. Liu, J. C. Mc, A. M. Killop, D. H. El-Zawahry, J. Y. Holman, W. D. Cheng, A. E. Meacham, A. F. Mahdy, L. S. Saad, et al. 2007. Role of acid ceramidase in resistance to FasL: therapeutic approaches based on acid ceramidase inhibitors and FasL gene therapy. *Mol. Ther.* **15**: 1259–1263.
34. Flowers, M., G. Fabrias, A. Delgado, J. Casas, J. L. Abad, and M. C. Cabot. 2012. C6-ceramide and targeted inhibition of acid ceramidase induce synergistic decreases in breast cancer cell growth. *Breast Cancer Res. Treat.* **133**: 447–458.
35. Gouazé-Andersson, V., M. Flowers, R. Karimi, G. Fabrias, A. Delgado, J. Casas, and M. C. Cabot. 2011. Inhibition of acid ceramidase by a 2-substituted aminoethanol amide synergistically sensitizes prostate cancer cells to N-(4-hydroxyphenyl) retinamide. *Prostate*. **71**: 1064–1073.
36. Mahdy, A. E., J. C. Cheng, J. Li, S. Elojeimy, W. D. Meacham, L. S. Turner, A. Bai, C. R. Gault, A. S. McPherson, N. Garcia, et al. 2009. Acid ceramidase upregulation in prostate cancer cells confers resistance to radiation: AC inhibition, a potential radiosensitizer. *Mol. Ther.* **17**: 430–438.
37. Morales, A., R. Paris, A. Villanueva, L. Llacuna, C. Garcia-Ruiz, and J. C. Fernandez-Checa. 2007. Pharmacological inhibition or small interfering RNA targeting acid ceramidase sensitizes hepatoma cells to chemotherapy and reduces tumor growth in vivo. *Oncogene*. **26**: 905–916.
38. Samsel, L., G. Zaidel, H. M. Drumgoole, D. Jelovac, C. Drachenberg, J. G. Rhee, A. M. Brodie, A. Bielawska, and M. J. Smyth. 2004. The ceramide analog, B13, induces apoptosis in prostate cancer cell lines and inhibits tumor growth in prostate cancer xenografts. *Prostate*. **58**: 382–393.
39. Szulc, Z. M., N. Mayroo, A. Bai, J. Bielawski, X. Liu, J. S. Norris, Y. A. Hannun, and A. Bielawska. 2008. Novel analogs of D-e-MAPP and B13. Part 1: synthesis and evaluation as potential anticancer agents. *Bioorg. Med. Chem.* **16**: 1015–1031.
40. Gangoiti, P., M. H. Granado, A. Alonso, F. M. Goni, and A. Gomez-Munoz. 2008. Implication of ceramide, ceramide 1-phosphate and sphingosine 1-phosphate in tumorigenesis. *Transl. Oncogenomics*. **3**: 81–98.
41. Ballereau, S., T. Levade, Y. Genisson, and N. Andrieu-Abadie. 2012. Alteration of ceramide 1-O-functionalization as a promising approach for cancer therapy. *Anticancer. Agents Med. Chem.* **12**: 316–328.
42. Itoh, M., T. Kitano, M. Watanabe, T. Kondo, T. Yabu, Y. Taguchi, K. Iwai, M. Tashima, T. Uchiyama, and T. Okazaki. 2003. Possible role of ceramide as an indicator of chemoresistance: decrease of the ceramide content via activation of glucosylceramide synthase and sphingomyelin synthase in chemoresistant leukemia. *Clin. Cancer Res.* **9**: 415–423.
43. Gouazé-Andersson, V., and M. C. Cabot. 2011. Sphingolipid metabolism and drug resistance in hematological malignancies. *Anticancer. Agents Med. Chem.* **11**: 891–903.
44. Kartal Yandim, M., E. Apohan, and Y. Baran. 2013. Therapeutic potential of targeting ceramide/glucosylceramide pathway in cancer. *Cancer Chemother. Pharmacol.* **71**: 13–20.
45. Li, H., and D. G. Tang. 2011. Prostate cancer stem cells and their potential roles in metastasis. *J. Surg. Oncol.* **103**: 558–562.
46. Chatelut, M., M. Leruth, K. Harzer, A. Dagan, S. Marchesini, S. Gatt, R. Salvayre, P. Courtoy, and T. Levade. 1998. Natural ceramide is unable to escape the lysosome, in contrast to a fluorescent analogue. *FEBS Lett.* **426**: 102–106.
47. Messner, M. C., and M. C. Cabot. 2010. Glucosylceramide in humans. *Adv. Exp. Med. Biol.* **688**: 156–164.
48. Shtraizent, N., E. Elyahu, J. H. Park, X. He, R. Shalgi, and E. H. Schuchman. 2008. Autoproteolytic cleavage and activation of human acid ceramidase. *J. Biol. Chem.* **283**: 11253–11259.
49. Oinonen, C., and J. Rouvinen. 2000. Structural comparison of Ntn-hydrolases. *Protein Sci.* **9**: 2329–2337.
50. Elyahu, E., N. Shtraizent, X. He, D. Chen, R. Shalgi, and E. H. Schuchman. 2011. Identification of cystatin SA as a novel inhibitor of acid ceramidase. *J. Biol. Chem.* **286**: 35624–35633.
51. Johnson, S. L., and M. Pellicchia. 2006. Structure- and fragment-based approaches to protease inhibition. *Curr. Top. Med. Chem.* **6**: 317–329.
52. Leung-Toung, R., Y. Zhao, W. Li, T. F. Tam, K. Karimian, and M. Spino. 2006. Thiol proteases: inhibitors and potential therapeutic targets. *Curr. Med. Chem.* **13**: 547–581.
53. Santos, M. M., and R. Moreira. 2007. Michael acceptors as cysteine protease inhibitors. *Mini Rev. Med. Chem.* **7**: 1040–1050.
54. Realini, N., C. Solorzano, C. Pagliuca, D. Pizzirani, A. Armirotti, R. Luciani, M. P. Costi, T. Bandiera, and D. Piomelli. 2013. Discovery of highly potent acid ceramidase inhibitors with in vitro tumor chemosensitizing activity. *Sci. Rep.* **3**: 1035.
55. Bielawska, A., J. Bielawski, Z. M. Szulc, N. Mayroo, X. Liu, A. Bai, S. Elojeimy, B. Rembiesa, J. Pierce, J. S. Norris, et al. 2008. Novel analogs of D-e-MAPP and B13. Part 2: signature effects on bioactive sphingolipids. *Bioorg. Med. Chem.* **16**: 1032–1045.
56. Bieberich, E. 2011. Ceramide in stem cell differentiation and embryo development: novel functions of a topological cell-signaling lipid and the concept of ceramide compartments. *J. Lipids*. **2011**: 610306.